Dual-Dynamic Interpenetrated Networks Tuned through Macromolecular Architecture

Journal:	*Polymer Chemistry*
Manuscript ID	PY-ART-09-2019-001387.R1
Article Type:	Paper
Date Submitted by the Author:	23-Oct-2019
Complete List of Authors:	Zhang, Borui; Miami University, Department of Chemistry and Biochemistry Ke, Jun; Miami University, Department of Chemistry and Biochemistry Vakil, Jafer; Miami University, Department of Chemistry and Biochemistry Cummings, Sean; Miami University, Department of Chemistry and Biochemistry Digby, Zachary; Miami University Sparks, Jessica; Miami University Ye, Zhijiang; Miami University Department of Mechanical and Manufacturing Engineering Zanjani, Mehdi; Miami University College of Engineering and Computing, Mechanical & Manufacturing Engineering Konkolewicz, Dominik; Miami University, Department of Chemistry and Biochemistry

SCHOLARONE™
Manuscripts

Dual-Dynamic Interpenetrated Networks Tuned through Macromolecular Architecture

Borui Zhang,[a] Jun Ke,[a] Jafer R. Vakil,[a] Sean C. Cummings,[a] Zachary A. Digby,[a] Jessica L. Sparks,[b] Zhijiang Ye,[c] Mehdi B. Zanjani,[c] Dominik Konkolewicz[a,*]

[a] Department of Chemistry and Biochemistry, Miami University, 651 E High St, Oxford OH, 45056, USA

[b] Department of Chemical, Paper and Biomedical Engineering, Miami University, 650 E High St, Oxford OH, 45056, USA

[c] Department of Mechanical and Manufacturing Engineering, Miami University, 650 E High St, Oxford, OH 45056, USA

Abstract

Recent progress on stretchable, tough dual-dynamic polymer single networks (SN) and interpenetrate networks (IPN) has broadened the potential applications of dynamic polymers. However, the impact of macromolecular structure on the material mechanics remains poorly understood. Here, rapidly exchanging hydrogen bonds and thermoresponsive Diels-Alder bonds were included into molecularly engineered interpenetrated network materials. RAFT polymerization was used to make well-defined polymers with control over macromolecular architecture. The IPN materials were assessed by gel permeation chromatography, differential scanning calorimetry, tensile testing and rheology. The mechanical properties of these IPN materials can be tuned by variation of the crosslinker content and chain length. All materials are elastic and have dynamic behavior at both ambient temperature and elevated temperature (90 °C), owing to the presence of the dual

dynamic noncovalent and covalent bonds. 100% self-healing recovery was achieved and a maximum stress level of up to 6 MPa was obtained. The data suggested the material's healing properties are inversely proportional to the content of the crosslinker or the degree of polymerization at both room and elevated temperature. The thermoresponsive crosslinker restricted deformation to some extent at ambient environment but gave excellent malleability upon heating. The underlying mechanism was explored by the computational simulations. Furthermore, a single network material with the same crosslinker content and degree of polymerization as the IPN was made. The SN was substantially weaker than the comparable IPN material.

Introduction

Dynamic chemistry (DC) is a powerful approach to make complex molecules and materials through the reversible reaction of simple building blocks under the thermodynamic control.[1] It has developed rapidly in the past decades and become an efficient tool in areas from drug discovery to materials science.[2] Particularly, dynamic materials (DM) or dynamers, which are polymeric materials containing dynamic bonds, have attracted great attention owning to their distinctive mechanical properties such as self-repaired ability, shape memory ability, malleability, and degradability.[3-7] Enhanced fracture toughness and multiple healing cycles can also be achieved due to the dynamic bonds. Dynamic noncovalent interactions, such as hydrogen bonds, hydrophobic interactions, host-guest interactions, zwitterionic interactions and metal-ligand coordination, often have fast exchange under ambient conditions. [3, 8-19] Dynamic covalent bonds, such as Diel-Alder adducts, disulfide bonds, imine bonds, acrylhydrazone bond and boronic-ester complexation, give relatively slow exchange and give better stability,

and are typically activated to exchange under external stimuli. (heat, pH or light)[20-45] Dynamers containing only one kind of dynamic bonds have the potential to creep or deform over time under load, owing to the dynamic nature of these reversible bonds, or be non-dynamic until an external stimulus is applied. Often, the materials that heal quickly also tend to creep rapidly.[6] However, the combination of dynamic and static bonds can be taken advantage of to overcome this limitation,[46-49] although the static bond could restrict the otherwise desirable dynamic properties. To address this limitation, materials possessing multiple orthogonal dynamic chemistries allows for the fine-tuning of a material response to multiple stimuli to achieve desired material properties.[50] Above all, developing the dynamers possessing different class of dynamic bonds will override those limitations, strengthen the advantages, and thereby broaden the fields of application of the dynamic polymeric materials.

Hydrogen bonding is observed in many biopolymers, such as the connective proteins in both soft and hard tissues, imparting the remarkable combination of strength and elasticity to the structures.[51, 52] Inspired by nature, polymers exploiting quadruple hydron bonding motifs have been extensively studied.[6, 53, 54] Specifically, the 2-(((6-(3-(6-methyl-4-oxo-1,4-dihydropyrimidin-2-yl)ureido)hexyl)carbamoyl)oxy)ethyl acrylate (UPyA) self-complementary end groups can form dimer units of a high association constant and establish the supramolecular polymers with a high degree of polymerization.[6, 55] UPyA linkages have also been shown to exchange efficiently in minutes at room temperature,[56] which enables the synthesis of tough and self-healable materials.[56, 57] Similarly, the reversible Diels-Alder reaction has been extensively used to develop self-healing materials.[7] It also belongs to the class of click reactions,[58] and it is well suited for

dynamic crosslinking applications since all atoms of the starting components are also present within the product, due to the 4+2 cycloaddition nature of the reaction.[6 21, 26, 59, 60] Also, the operation of the Diels-Alder reaction is simple as it is highly resistant to water and oxygen. This paper reports novel self-healing double dynamers containing both dynamic hydrogen bonds from the 2-ureido-4[1H]-pyrimidinone (UPy) moiety in one chain and covalent bonds from Diels-Alder adducts in the other chain, with exceptional control over the underlying polymer structure. Earlier work used conventional free radical polymerization to synthesize these materials, leading to poor control over the underlying polymer's structure and consequently the properties of materials. Macromolecular architecture is an important tool for tuning material properties, yet relatively limited information is known on the impact of polymer structure and architecture on the properties of dynamic and self-healing materials.[61] This contribution explores the impact of macromolecular architecture on dynamic materials containing both dynamic hydrogen bonded and dynamic covalent linkers.

Reversible addition-fragmentation chain-transfer (RAFT) polymerization has been extensively used to synthesize a wide variety of polymeric materials.[62-66] RAFT polymerization, which controls the polymer's structure using a thiocarbonylthio based chain transfer agent (CTA), can be used with a wide range of monomers and reaction conditions and meanwhile provide controlled molecular weight polymers with narrow dispersities. (usually $M_w/M_n < 1.20$; sometimes $M_w/M_n < 1.10$)[67] In addition, its versatility and ability to create well defined polymers from a wide range of functional monomers make it a powerful and popular tool to develop new materials by combining RAFT and dynamic chemistry. This can lead to the development of multiply responsive functional polymeric materials with diverse

macromolecular architectures.[49, 68-71] In this paper, RAFT polymerization was used to synthesize polymers to control and tune underlying macromolecular architectures.

The combination of noncovalent and covalent chemistry has been used in both single networks (SN) and interpenetrating networks (IPN) over the past few years.[5, 8, 46, 48-50, 59, 72-78] Specially, interpenetrating networks (IPNs) have received significant interest because their unique architecture can dramatically enhance the mechanical properties of the dynamic materials. This structure has been utilized to make various of functional materials so far. In 2017, Wang *et al.* produced an injectable IPN incorporating boronate ester bonds in one polymer and acylhydrzone bonds in the other.[79] The tunable mechanical properties and self-healing abilities can be controlled by polymer concentration and pH values. This research opened a new perspective on creating responsive 3D-printable bio-ink materials. In 2018, Tang *et al.* developed the thermally healable double-network ion gels which is composed of dynamic crosslinked P(FMA-co-MMA) and physically crosslinked P(VDF-co-HFP) networks with ionic liquid.[80] Failure tensile stress 660 kPa and strain 268% were obtained. This gel possesses an ionic conductivity of 3.3 mS cm^{-1} at room temperature. This smart gel has potential to be a component of the flexible electronics. In 2019, Zhou *et al.* reported a dynamic IPN strategy to make multiresponsive reversible wrinkle.[81] The wrinkle layer was constructed with the anthracene-containing polymers PAN and disulfide containing DSDA monomer. The resulted wrinkle offers a promising application in smart display.

Among all the aforementioned studies, the impact of macromolecular structures on the material mechanics remains poorly understood. Our group's previous study in 2017, investigated the structural configuration of SN and IPN dynamic materials

and the influence of different compositions on the properties of materials.[48] Specifically, each network in the SN and IPN materials containing dynamic bonds made by free radical polymerization,[48] and studied through molecular dynamics simulations.[82] However, the degree of polymerization and the macromolecular architecture cannot be regulated precisely using conventional free radical polymerization. Moreover, the preparation of FMIDA crosslinker has several intricate steps. The failure tensile stress of the free radical polymerized material is only around 600 kPa. To address these, here, we report RAFT polymerized bulk state dynamic materials containing poly(ethyl acrylate) (PEA) as the main backbone with a UPyA crosslinkers based on either an acrylic (UPyA) or methacrylic (UPyMA) based hydrogen bonded linkers and furfuryl methacrylate (FMA) crosslinkers. The FMA units can be obtained through one-pot reaction with decent purity. It is easy to dissolve and can be crosslinked using a bismaleimide compound. The RAFT process allows fine tuning of the crosslinker content and the polymer chain length of the PEA-UPyA-FMA based SN and IPN materials. The PEA_{100}-$UPyMA_{3.75}$-$FMA_{3.75}$ SN as a representative was synthesized by RAFT polymerization to compare the material properties with the IPN. This paper explores the impact of macromolecular architecture on the mechanical, self-healing and malleability properties. 100% self-healing recovery was achieved and a maximum tensile stress of 6 MPa was obtained.

Experimental section

Materials

Unless otherwise noted, all materials, reagents, and solvents were purchased from commercial sources and used as received without further purification.

Synthesis of 1-(6-isocyanatohexyl)-3-(6-methyl-4-oxo-1,4-dihydropyrimidin-2-yl)urea (UPyNCO)

The synthesis of UPy-NCO was adapted from literature.[83] To a round bottom flask equipped with a magnetic stirrer bar, 2-amino-4-hydroxy-6-methylpyrimidine (11.19 g, 0.0895 mol) and 1,6-hexadiisocyanate (108.50 g, 0.6460 mol) were added. The reaction mixture was capped with a rubber septum and purged with nitrogen for 10 min. Anhydrous pyridine (7.82 g, 0.0989 mol) was added via syringe and the reaction mixture was heated at 100 °C for 16 h. To this reaction mixture 30 ml of hexane was added and the precipitates were washed by diethyl ether. The white solid was dried under reduced pressure to give UPy-NCO (25.72 g, 0.0877 mol, 98% yield). The compound was confirmed by ^{1}H-NMR in agreement with the literature.[83] ^{1}H-NMR (300 MHz, CDCl$_3$) δ ppm 13.10 (s, 1H), 11.86 (s, 1H), 10.17 (s, 1H), 5.82 (s, 1H), 3.28 (m, 4H), 2.23 (s, 3H), 1.62 (quin, J = 6.9 Hz, 4H), 1.41 (m, 4H).

Synthesis of 2-(((6-(3-(6-methyl-4-oxo-1,4-dihydropyrimidin-2-yl)ureido)hexyl)carbamoyl)oxy)ethyl acrylate (UPyA)

The prepared UPy-NCO (6.98 g, 0.0238 mol) was added to a round bottom flask containing a magnetic stirrer bar, followed by adding 105 mL of chloroform, 2-hydroxyethyl acrylate (HEA) (6.90 g, 0.059 mol) and 3 drops of dibutyltin dilaurate (DBTDL). The reaction mixture was heated at 65 °C for 16 h. After the reaction, the solids were removed by filtration and a large excess of diethyl ether was added to generate a white precipitate. The precipitate was collected by vacuum filtration and washed with diethyl ether, hexane and again by diethyl ether. The solid was dried to give the UPyA product (8.68 g, 0.0211 mol, 89% yield). The compound was confirmed by ^{1}H-NMR in agreement with the literature.[46] ^{1}H-NMR (300 MHz, CDCl$_3$) δ ppm 13.17 (s, 1H), 11.90 (s, 1H), 10.16 (s, 1H), 6.43 (d, J = 15.9 Hz, 1H), 6.14 (m,

1H) 5.85 (m, 2H), 4.97 (br, 1H), 4.32 (m, 4H) 3.25 (quart, *J* = 5.8 Hz, 2H), 3.17 (m, 2H), 2.23 (s, 3H), 1.62 (m, 2H), 1.51 (m, 2H), 1.41 (m, 4H).

Synthesis of 2-(((6-(3-(6-methyl-4-oxo-1,4-dihydropyrimidin-2-yl)ureido)hexyl)carbamoyl)oxy)ethyl methacrylate (UPyMA)

UPy-NCO (6.98g, 0.0238 mol) was added to a round bottom flask equipped with a magnetic stirrer bar. To this solid, 105 mL of chloroform, hydroxyethyl methacrylate (14.35 mL, 15.36 g, 0.1180 mol) and 3 drops of dibutyltindilaurate were added. The mixture was then homogenized and heated at 65 °C for 16 h. The solids were then removed by filtration. Diethyl ether was used in excess to yield a white precipitate, which was collected via vacuum filtration and washed with diethyl ether, hexane, and diethyl ether again. The solid was dried to yield the UPy-MA product. The compound was confirmed by ^{1}H-NMR in agreement with the literature.[84] ^{1}H-NMR (300 MHz, CDCl$_3$) δ ppm 13.13 (s, 1H), 11.86 (s, 1H), 10.07 (s, 1H), 6.14(m, 1H) 5.86 (m, 1H), 5.60 (m, 1H), 5.00 (br, 1H), 4.32(m, 4H) 3.25 (quart, *J* = 5.8 Hz, 2H), 3.17 (m, 2H), 2.23 (s, 3H), 1.94 (s, 3H), 1.62 (m, 2H), 1.58 (m, 2H), 1.50 (m, 4H).

Synthesis of furfuryl methacrylate (FMA)

Furfural alcohol (6.00 g, 0.0612 mol) and *N,N*-dimethylaminopyridiene (DMAP, 3.73 g, 0.0305 mol) were added to a round bottom flask containing a magnetic stirrer bar, and to these solids 70 mL of DCM and methacrylic acid (6.30 g, 0.0734 mol) were added. The reaction mixture was cooled to 0 °C, and 1-(3-dimethylaminopropyl)-3-ethylcarbodiimide hydrochloride (EDC, 22.00 g, 0.1148 mol) was added. The solution was allowed to warm to room temperature and stirred for 24 h at room temperature. After the reaction, the DCM phase was washed with 0.2 M hydrochloride (6 × 150 mL), followed by brine (1 × 150 mL), 0.1

M sodium hydroxide (3 × 150 mL), deionized water (1 × 150 mL) and again brine (1 × 150 mL). The solvent was removed under reduced pressure to give desired FMA product which is light yellow oil (3.78 g, 0.0227 mol, 37% yield). The compound was confirmed by ^{1}H-NMR in agreement with the literature.[85] ^{1}H-NMR (300 MHz, CDCl$_3$) δ ppm 7.42 (s, 1H), 6.42 (d, J = 3.2 Hz, 1H), 6.40-6.33 (m, 1H), 6.13 (s, 1H), 5.57 (s, 1H), 5.13 (s, 2H), 1.94 (s, 3H).

Synthesis of (2-propionic acid)yldodecyl trithiocarbonate (PADTC)

(2-propionic acid)yldodecyl trithiocarbonate (PADTC) was synthesized following the literature, and the product was confirmed by the ^{1}H-NMR in agreement with the literature.[86, 87] ^{1}H-NMR (500 MHz, CDCl$_3$) δ (ppm) 4.87 (quin, J = 7.4 Hz, 1H), 3.36 (t, J = 7.4 Hz, 2H), 1.70 (quin, J = 7.4 Hz, 2H), 1.63 (d, J = 7.4 Hz, 3H), 1.40 (br quin, J = 7.2 Hz, 2H), 1.26 (br, 16H), 0.88 (t, J = 6.9 Hz, 3H).

**RAFT polymerization of PEA-UPyA polymer**

The series of synthesized PEA-UPyA is shown in Table S1. Synthesis of PEA$_{100}$-UPyA$_5$, used as an example, demonstrates the general procedure of RAFT polymerization. To a 50 mL round bottom flask containing a magnetic stirrer bar, UPyA powder (1.0259 g, 0.0025 mol) and 8.3300 g Dimethylformamide (DMF) were added. The reaction mixture was capped with a rubber septum, and then homogenized at 65 °C, followed by deoxygenate with nitrogen for 20 min at ambient temperature. Meanwhile, PADTC (0.1751 g, 0.0005 mol), azobisisobutyronitrile (AIBN, 0.0164 g, 0.0001 mol), ethyl acrylate (EA, 5.0000 g, 0.0499 mol) and 1.0000 g DMF were added in a small vial and deoxygenated. The prepared reaction mixture in the small vial was transferred to the round bottom flask via syringe, while the whole system was still being purged with nitrogen. The reaction was stirred at 65 °C overnight. The resulting PEA$_{100}$-UPyA$_5$ polymer solution was confirmed by 500 MHz ^{1}H-NMR

with above 95% conversion. The materials were analyzed by gel permeation chromatography (GPC) to evaluate molecular weight distributions and NMR spectroscopy to estimate the units of EA and UPyA moieties in the polymer. The data are shown in both Table S1 and S2.
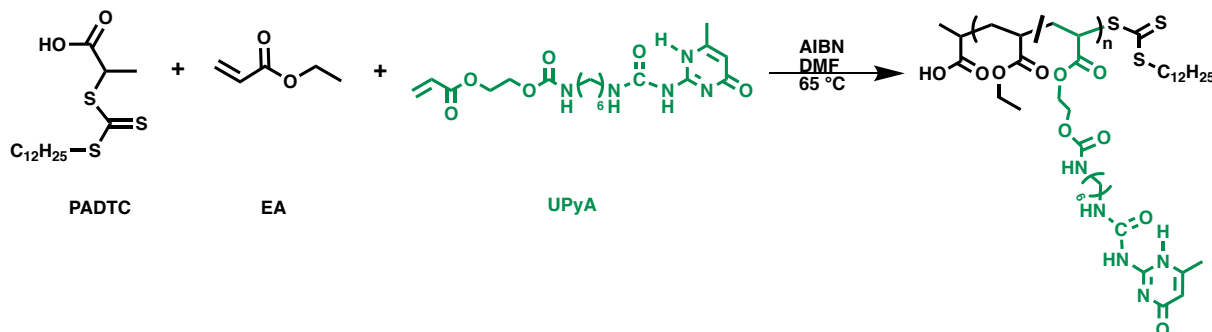
RAFT polymerization of PEA-FMA polymer

The series of synthesized PEA-FMA is shown in Table S3. Synthesis of PEA_{100}-FMA_5, used as an example, states the general procedure of synthesizing PEA-FMA polymer. To a 50 mL round bottom flask equipped with a magnetic stirrer bar, PADTC (0.1751 g, 0.0005 mol), AIBN (0.0164 g, 0.0001 mol), EA (5.0000 g, 0.0499 mol), FMA (0.4149 g, 0.0025 mol) and 8.4100 g toluene were added. The reaction mixture was capped with a rubber septum and purged with nitrogen for 20 min. The reaction was stirred at 65 °C for 5 h. The resulting PEA_{100}-FMA_5 polymer solution was confirmed by 500 MHz ^{1}H-NMR with above 85% conversion. The crude product was precipitated by dropwise addition to the stirred hexane. The product was dried in a vacuum oven giving PEA_{100}-FMA_5. The materials were analyzed by GPC to evaluate molecular weight distributions and NMR spectroscopy to calculate the units of EA and FMA. The data are shown in Table S4.
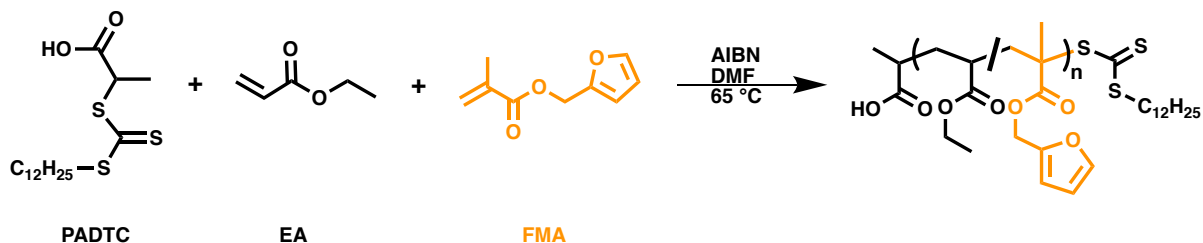
General procedure for making PEA-UPyA-FMA interpenetrated networks (IPN)

PEA_{100}-FMA_5-$UPyA_5$ is used here as an example to demonstrate the general procedure of making interpenetrated networks. The prepared dry PEA_{100}-FMA_5 polymer was weighed and the mass (4.70 g, 0.0004 mol) was taken to calculate the theoretical weight of PEA_{100}-$UPyA_5$ polymer DMF solution, in order to combine two polymers as 1:1 ratio in respect to polymer weight. In this case, 11.74 g PEA_{100}-$UPyA_5$ polymer DMF solution was taken to precipitate by dropwise addition to the other Erlenmeyer flask containing the stirred ethyl ether. Then the solvent was drained and another 9.40 g DMF was added to redissolve the precipitates via sonicator. The new-made PEA_{100}-$UPyA_5$ polymer DMF solution was combined with the prepared dry PEA_{100}-FMA_5 polymer and homogenized via sonicator. In a separate vial, 1,1'-(Methylenedi-4,1-phenylene)bismaleimide (BMI) (0.46 g, 0.0013 mol) was dissolved in 3.00 g of DMF and, then transferred into the flask containing the prepared polymer mixture solution. Once fully dissolved, the contents of the flask were transferred to a Teflon mold to process polymerization at 50-55 °C for 48 h. After crosslinking, the materials were removed from the Teflon mold and allowed to dry in the fume hood for 2 days and overnight in a vacuum oven.

Synthesis and development of PEA_{100}-$UPyMA_{3.75}$-$FMA_{3.75}$ Single networks (SN)

To a round bottom equipped with a magnetic stirrer bar, ethyl acrylate (5.00 g, 0.0499 mol), FMA (0.2490 g, 0.0015 mol), UPy-MA (0.6341 g, 0.0015 mol), PADTC (0.1401 g, 0.0004 mol), AIBN (0.0066 g, 0.00004 mol), and DMF (10.00 g, 0.1368

mol) were added. The reaction mixture was capped with a rubber septum and purged with nitrogen for 10 min. The mixture was heated at 60 °C for 8 h. The reaction was then pushed to 75-80% conversion, confirmed by ^{1}H-NMR. To an Erlenmeyer flask, 50 mL of diethyl ether and 50 mL of hexanes was added. The polymer in the round bottom was then precipitated in the Erlenmeyer flask. Excess solvent was discarded, and the flask was then dried in a vacuum oven. The polymer was then dissolved in 6.0000 g DMF, and 1,1'-(Methylenedi-4,1-phenylene) bismaleimide (0.3221 g, 0.0009 mol) was dissolved in 2.0000 g DMF. The BMI solution was then homogenized with the dissolved polymer. The resulting mixture was then transferred to the Teflon molds and heated at 50-55 °C for 48 h. After the polymer had crosslinked, the materials were removed out from Teflon molds and allowed to dry in the fume hood for 2 days and overnight in a vacuum oven.

Characterization Methods

All nuclear magnetic resonance (NMR) were determined in $CDCl_3$ with a Bruker 300 or 500 MHz spectrometer. Infrared (IR) spectroscopy was performed on a PerkinElmer Spectrum 100 Spectrometer.

Differential scanning calorimetry (DSC)

Differential scanning calorimetry (DSC) study was performed on a TA Instruments Q20 system, with a heat-cool-heat cycle ranging from -40 °C to +195 °C at a heating rate of 10 °C min^{-1}. Only data from the second heating cycle was used for analysis. The glass transition temperature (T_g) was identified from the inflection point determined as the minimum in the first derivative. The first derivative was smoothed using a 5-point average.

Gel permeation chromatography (GPC)

Polymer molecular weights and dispersity were determined using an Agilent 1260 SEC system equipped with an autosampler, an Agilent 1260 isocratic pump, Agilent 1 guard and 2 analytical Polar Gel-M columns, degasser, and Agilent 1260 refractive index (RI detector) and a viscometer for universal calibration. *N,N*-Dimethylformamide (DMF) + 0.1 wt% LiBr was used as the eluent with a flow rate of 1 mL min^{-1} at 50 °C. Each sample was filtered before injection. The SEC system was calibrated with poly(methyl methacrylate) standards.

Tensile testing

An Instron 3344 universal testing system equipped with a 100 N load cell was used to perform tensile testing of the materials at ambient temperature to obtain stress-strain curves. The extension was increased at the rate of 1 mm s^{-1} and all samples were measured until the material broke. Each tensile test was repeated at least 5 times.

Cutting and healing procedures

Materials were cut into half with a razor blade and then the resulting two halves were placed in contact together. The reattached materials were placed either in a preheated oven at 90 °C or on a non-stick pan at ambient temperature to heal for different time periods.

Stress relaxation Test

An Instron 3344 apparatus equipped with a 100 N load cell was used to analyze stress relaxation at ambient environment. The extension was increased at the rate of 0.5 mm s^{-1} until 25% average strain at break of each material was achieved. The strain was maintained while the stress was measured over a 4 h period.

Creep Experiments

An DMA Q800 instruments was used to analyze creep deformation at 30 °C. All the creep experiments were performed with the material being extended until a stress of 50 kPa was achieved, except PEA_{100}-$UPyA_5$-FMA_5 IPN which was used 25 kPa. The constant stress was hold for 1 h and then released. The strain recovery was measured for the following 2 h.

Rheology

A TA instruments Discovery HR-1 rheometer was used for rheological studies. A 20 mm crosshatched parralel plate geometry was used at 0.1% applied strain for rheological frequency sweeps. 0.1 Hz frequency was used for the temperature sweep.

Young's modulus Calculation

An incompressible Ogden hyperelastic constitutive law[88] (eqn (1)) was used to model the tensile response of the materials.

$$\sigma_{\text{eng}} = \frac{2G}{\alpha}\left[\lambda^{\alpha-1} - \lambda^{-1-\left(\frac{\alpha}{2}\right)}\right] \tag{1}$$

σ_{eng} is the engineering stress. α is the strain hardening exponent. G is the shear modulus, and λ is the stretch ratio. G and α were found for each sample by fitting eqn (1) to the experimental mechanical data. Eventually, elastic modulus (E) was found from eqn (2).

$$E = 2G(1 + v) \tag{2}$$

Where v represents Poisson's ratio (assumed to be 0.5 for an incompressible material). Mean values of the Young's modulus for each material is given in Table 2. Fitted Young's modulus curve for each material is given in Figure S1.

Reshaping materials

The materials were twisted 360°, followed by the placement of two clips on either side of the materials. The materials with the fixed new configuration were heated at 90 °C. After heating different time periods, the materials were released and allowed to completely relax. The resulting angle between the two ends of each material was measured.

Long-term stability and creep recovery

A material was taken and its length was measured, followed by stretching to 25% average strain at break and fixed at that strain in ambient environment. After 24 h, the strain was released and the material length was measured after different time periods. Comparing with the original length of the material, the creep recovery can be obtained.

Results and discussion

Synthesis of Polymers for IPN Materials

RAFT polymerization was used to create well defined polymers. Ethyl Acrylate (EA) was used as the backbone forming monomer. Two independent crosslinked networks entangle with each other in IPN materials as shown in Scheme 1. One network contains hydrogen bonding from UPyA dimers, giving noncovalent interactions. The second network is crosslinked by adding 1,1'-(Methylenedi-4,1-phenylene)bismaleimide (BMI) to form the thermoresponsive Diels-Alder adducts, giving dynamic covalent interactions. Each polymer's composition, number average molecular weight and the dispersity was collected in Table S1-S4. The macromolecular chain length, and crosslinker density of PEA-UPyA-FMA IPN materials were varied to investigate the impact of macromolecular architecture on the material properties.

IPN materials were prepared by synthesizing polymers containing either UPyA or FMA based crosslinkers. 3 primary chain lengths based on ethyl acrylate (EA) content (50 units, 100 units or 150 units) were synthesized with 7.5mol% crosslinker in each chain, as well as 3 distinct crosslink densities (5mol%, 7.5mol%, or 10mol%) with primary chain length of 100 were synthesized using RAFT polymerization. Applying the probability analysis of Harrisson et al.[89] suggests that a chain with 3.75 units of crosslinker (PEA$_{50}$-UPyA$_{3.75}$ and PEA$_{50}$-FMA$_{3.75}$) should have less than 2.5% of chains with no crosslinker, and less than 12% of chain with zero or one crosslinker. As the crosslinker loading is increased the fraction of chains without a crosslinker decreases, and with 11.25 units of crosslinker (PEA$_{50}$-UPyA$_{11.25}$ and PEA$_{50}$-FMA$_{11.25}$) the probability of a chain having zero or one crosslinker is below 0.02%. In these IPN materials, the subscript of PEA in this paper refers to the desired chain length of each polymer chain and the subscript of UPyA or FMA refers to the desired molar content of each crosslinker in a polymer chain. All polymers were well controlled with narrow disperties as indicated in Table S1-4. The properties of the resulting polymers are given in Table 1. In general, the polymers molecular weights obtained from the analysis of NMR agreed well with the theoretical values, and the polymers had disperities (M_w/M_n values) below 1.25, indicating well controlled polymers. It was found that the molecular weight of the PEA-UPyA obtained from GPC (Table S1) was not in agreement with their theoretical molecular weight. We speculated that this was because the PEA-UPyA assembled on the GPC column we were using, thus were hard to elute. Therefore, the NMR was also used to calculate the molecular weight. The GPC traces of with PEA$_{50}$-UPyA$_{3.75}$ and PEA$_{50}$-FMA$_{3.75}$ gave the evidence of the impact of the RAFT on manipulating the desired polymers' structures. (Figure S2). IPN materials were

prepared by dissolving both individual polymers in DMF, combining them and adding BMI to crosslink pendant furan units as shown in Scheme 1.
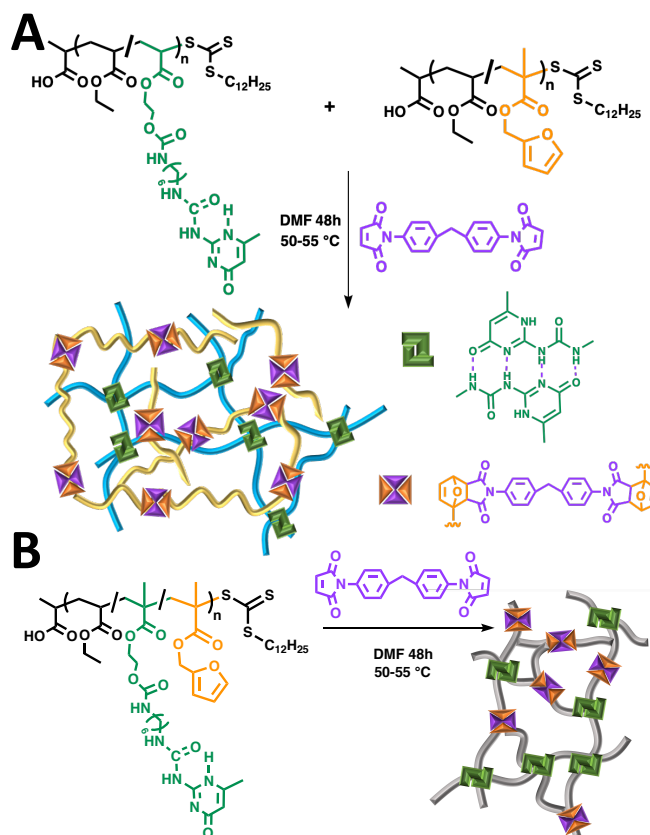
Scheme 1. Crosslinkers and polymers used in the preparation of RAFT based IPN (A) and SN (B) materials. Slashes indicate random incorporation of monomers.

All polymers were thoroughly dried after crosslinking. Five RAFT based interpenetrated networks (IPN) are reported based on the polymers. (entries 1-10 in Table 1). The PEA_{100}-$UPyA_5$-FMA_5, PEA_{100}-$UPyA_{7.5}$-$FMA_{7.5}$ and PEA_{100}-$UPyA_{10}$-FMA_{10} possess the same degree of polymerization (DP) but have different contents of crosslinkers. In contrast, PEA_{50}-$UPyA_{3.75}$-$FMA_{3.75}$, PEA_{100}-$UPyA_{7.5}$-$FMA_{7.5}$ and PEA_{150}-$UPyA_{11.25}$-$FMA_{11.25}$ contain 7.5% molar ratio of the crosslinkers but with different degree of polymerization, or primary chain lengths.

Table 1: Properties of polymers used to synthesize IPN materials. [a] Calculated by NMR, [b] calculated by GPC.

Entry	Polymer	$M_{n,theory}$	M_n[a]	M_w/M_n[b]	Units UPyA[a]	Units FMA[a]

1	$PEA_{100}\text{-}UPyA_5$	12398	12400	1.17	5.0	0
2	$PEA_{100}\text{-}UPyA_{7.5}$	13422	14900	1.13	7.4	0
3	$PEA_{100}\text{-}UPyA_{10}$	14445	16500	1.21	13.0	0
4	$PEA_{50}\text{-}UPyA_{3.75}$	6886	9530	1.17	5.3	0
5	$PEA_{150}\text{-}UPyA_{11.25}$	19957	22600	1.16	10.5	0
6	$PEA_{100}\text{-}FMA_5$	11182	11000	1.05	0	5.5
7	$PEA_{100}\text{-}FMA_{7.5}$	11597	11200	1.05	0	7.6
8	$PEA_{100}\text{-}FMA_{10}$	12013	11300	1.06	0	10.2
9	$PEA_{50}\text{-}FMA_{3.75}$	5974	6670	1.08	0	5.2
10	$PEA_{150}\text{-}FMA_{11.25}$	17221	21600	1.09	0	13.0
11	$PEA_{100}\text{-}UPyMA_{3.75}\text{-}FMA_{3.75}$	18726	13000	1.34	3.78	4.39

Characterizing IPN materials

Tensile testing, differential scanning calorimetry (DSC) and rheological studies were used to evaluate the fundamental properties of the PEA-UPyA-FMA IPN materials. All the vacuum-dried materials were placed into the hot oven at 90 °C for 24 h before performing any mechanical tests. This removed any residual DMF, and promoted the equilibration of the Diels-Alder adducts.

Tensile tests were carried out under ambient temperature for all uncut materials with typical stress strain curves given in Figure 1. The variability of typical stress - strain curves of all uncut materials can be found in Figure S3-S7. The average peak stress and strain at break were investigated based on crosslinker density and degree of polymerization, as shown in Figure 1A and 1B respectively. It was found that the molar ratio of crosslinker density is directly correlated with the material's peak stress (σ_{peak}), which is close to the stress at break. Also, at higher crosslink densities the materials show a decrease in the strain at break (ε_{break}). This is presumably due to the higher crosslink density greatly increasing the number of

elastically effective linkers, while decreasing the elasticity of the material due to increased net point density. With a primary backbone length of 100 units, as the contents of the crosslinkers is increased, the peak stress of the materials increases. Interestingly, the material with a shorter chain length, the PEA_{50}-$UPyA_{3.75}$-$FMA_{3.75}$, reaches a higher stress than the PEA_{100}-$UPyA_5$-FMA_5. This is likely because the PEA_{50}-$UPyA_{3.75}$-$FMA_{3.75}$ has a higher molar crosslink density than the PEA_{100}-$UPyA_5$-FMA_5 material leading to a greater density of crosslinking points.

Further, the strain at break of the materials is affected by the degree of polymerization. At the same crosslinker density, as the degree of polymerization is increased, the strain at break decreases and the peak stress increases. This is likely due to an increase in the number of elastically effective crosslinkers which percolate the polymer network, leading to an increase in the effective crosslink density in the material. For instance, PEA_{150}-$UPyA_{11.25}$-$FMA_{11.25}$ and PEA_{100}-$UPyA_{10}$-FMA_{10} were very rigid and relatively brittle, due to a large number of crosslinked points effective in the network compare to materials with lower crosslink densities. In general, materials with higher crosslink densities have lower strain at break and but can hold higher stress. This is reflected in the Young's modulus through the incompressible Ogden hyperelastic constitutive law.[88] Fitted Young's modulus curves for each IPN material are shown in Figure S1. Except the PEA_{100}-$UPyA_{10}$-FMA_{10} IPN, all the other typical stress-strain curves of each IPN material have an excellent Young's modulus fit and the PEA_{100}-$UPyA_{10}$-FMA_{10} IPN has an acceptable fit to the Ogden model. As indicated in Table 1, PEA_{100}-$UPyA_{10}$-FMA_{10} has the largest Young's modulus of 20000 ± 2000 kPa and PEA_{100}-$UPyA_5$-FMA_5 has the lowest Young's modulus of 340 ± 30 kPa among all five IPN materials. Therefore, a factor of 4 change in crosslink density leads to an almost 2 order of magnitude change in

Young's modulus. As with ε_{break} and σ_{peak}, higher crosslink densities or longer chain lengths dramatically increase Young's modulus, again through an increase in the effective crosslink density leading to a greater resistance to tensile deformation.
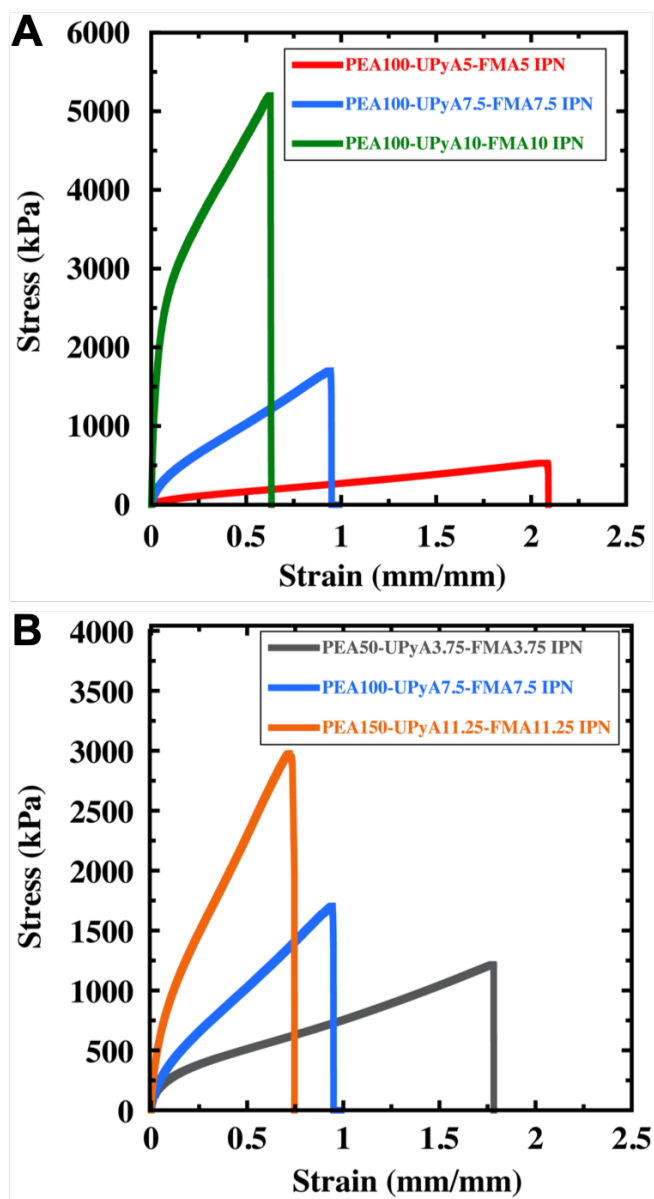

Figure 1. (A) Typical stress-strain curves of 100 DP IPN materials with different crosslinker content. (B) Typical stress-strain curves of IPN materials containing same molar ratio of crosslinkers with different DP.

Figure S8 gives the infrared (IR) spectrum of the PEA$_{100}$-UPyA$_5$-FMA$_5$ IPN material after it has been prepared and dried in the vacuum oven, which is typical of these

materials. The assigned peaks can be found in Table S5. The IR spectra of the other four IPN materials are similar to the PEA$_{100}$-UPyA$_5$-FMA$_5$ IPN material. The glass transition temperature of the materials was measured by differential scanning calorimetry (DSC). As shown in Table 2 (entry 1, 2 and 3), as the crosslinker content increases, the glass transition temperature (T_g) increases from approximately T_g = -5.42 °C for the PEA$_{100}$-UPyA$_5$-FMA$_5$ IPN to the approximately T_g = 1.68 °C for the PEA$_{100}$-UPyA$_{10}$-FMA$_{10}$ IPN. As the chain length increases, the T_g increases from approximately T_g = -7.81 °C for the PEA$_{50}$-UPyA$_{3.75}$-FMA$_{3.75}$ to the approximately T_g = -1.97 °C for the PEA$_{150}$-UPyA$_{11.25}$-FMA$_{11.25}$, shown in Table 2 (entry 2, 4 and 5). This is presumably due to a higher crosslinker density and longer chain length restricting the mobility and rotation of polymers, thus more thermal energy is needed to make the backbone relax. Raw DSC traces are given in Figure S9. Each of the five materials have a relatively low T_g which is well below room temperature. Therefore, each material should be relatively soft, and capable of dynamic exchange and self-healing under both ambient conditions and at elevated temperature.

Table 2. Properties of PEA-UPyA-FMA IPN materials — degree of polymerization (DP), net crosslinker density to the EA monomer, peak stress, strain at break, glass transition temperature (T_g) and Young's modulus. Errors represent a standard error based on 5 measurements.

IPN Materials	DP	Net UPy density	Net FMA density	σ_{peak} (kPa)	ε_{break} (mm/mm)	T_g (°C)	Young's modulus (kPa)
PEA$_{100}$-UPyA$_5$-FMA$_5$	100	0.025	0.025	460±50	1.8±0.3	-5.42	340±30
PEA$_{100}$-UPyA$_{7.5}$-FMA$_{7.5}$	100	0.0375	0.0375	1800±200	1.0±0.1	-2.87	2760±70
PEA$_{100}$-UPyA$_{10}$-FMA$_{10}$	100	0.05	0.05	5200±600	0.6±0.2	1.68	20000±2000
PEA$_{50}$-UPyA$_{3.75}$-FMA$_{3.75}$	50	0.0375	0.0375	1220±50	1.8±0.2	-7.81	1210±80
PEA$_{150}$-UPyA$_{11.25}$-FMA$_{11.25}$	150	0.0375	0.0375	2700±500	0.7±0.2	-1.97	7400±200

In addition to the properties summarized in Table 2, rheological studies were performed on all five PEA-UPyA-FMA IPN materials. Strain sweep experiments at 0.1 Hz showed that 0.1% strain is in the linear viscoelastic region for each material. The typical strain sweep curve is shown in Figure S10. Frequency sweep using 0.1%

strain were performed at room temperature. As indicated in Figure S11-S15, PEA_{100}-$UPyA_5$-FMA_5, PEA_{100}-$UPyA_{7.5}$-$FMA_{7.5}$ and PEA_{50}-$UPyA_{3.75}$-$FMA_{3.75}$ IPN materials had a similar storage and loss moduli that continuously increased with increasing frequency. This is consistent with materials that are close to their gel point and observed in other dynamic covalent cross-linked materials.[90, 91] However, PEA_{100}-$UPyA_{10}$-FMA_{10} and PEA_{150}-$UPyA_{11.25}$-$FMA_{11.25}$ IPN had higher storage modulus compared to the loss modulus, which is presumably due to the higher density of elastically effective crosslink density in these materials. It was also noted that all five samples had a similar rate of increase of storage and loss moduli, due to the relatively higher densities of crosslinkers and restricted chain mobility.

Similarly, to the Young's modulus, the shear modulus increased with crosslink density and with chain length, again due to a larger number of elastically effective net points at higher density of UPyA and FMA and longer chain lengths. When considering crosslink density, the PEA_{100}-$UPyA_5$-FMA_5 material had a higher Tanδ, especially at high frequency, and lower storage modulus than PEA_{100}-$UPyA_{7.5}$-$FMA_{7.5}$ with PEA_{100}-$UPyA_{10}$-FMA_{10} having the highest storage modulus and lowest Tanδ. This suggests that the lower crosslink density lead to increased chain relaxation due to lower entanglements and rigidification by crosslinking. Conversely, shorter chain lengths caused lower storage moduli but also higher Tanδ values, with the PEA_{50}-$UPyA_{3.75}$-$FMA_{3.75}$ material having a lower storage modulus and higher Tanδ than PEA_{100}-$UPyA_{7.5}$-$FMA_{7.5}$ and PEA_{150}-$UPyA_{11.25}$-$FMA_{11.25}$ having the highest storage modulus and lowest Tanδ. This is presumably due to a larger density of elastically effective crosslinks and chain entanglements at higher chain

length compared to the short chains, even though all these samples have the same net crosslink density.

Temperature sweep rheology was performed using 0.1% strain and 0.1 Hz on all IPN materials in the range from 20 °C to 150 °C. Figure 2 gives the temperature sweep rheological data of storage and loss modulus. As expected, the storage and loss moduli decreased at higher temperatures, and the materials transitioned from an elastic-like behavior at 20 °C to a rubbery-like material at intermediate temperatures, eventually reaching viscous-like behavior at elevated temperature for all materials except PEA_{150}-$UPyA_{11.25}$-$FMA_{11.25}$. The viscoelastic behavior of all five IPN materials are consistent with other dynamically crosslinked polymers with a dissociative dynamic bond exchange mechanism.[92, 93] This is because at elevated temperature the Diels-Alder equilibrium favors the dissociated form, leading to a major decrease in crosslink density which correlates to a sharp decrease in storage modulus. All materials showed a rubbery plateau in the approximate temperature range of 60-120 °C, with an essentially flat storage modulus which is substantially higher than the loss modulus. Except the PEA_{150}-$UPyA_{11.25}$-$FMA_{11.25}$ IPN materials, the other four IPN materials had a crossover point between storage modulus and loss modulus, beyond which the loss modulus exceeded the storage modulus. This indicates that the viscous response prevails, suggesting that the materials have turned into liquid-like polymers due to decrosslinking of FMA-BMI adducts. This is consistent with the melting of disk samples after being heated to 150 °C. Each approximate temperature at the crossover points of PEA_{100}-$UPyA_5$-FMA_5, PEA_{100}-$UPyA_{7.5}$-$FMA_{7.5}$, PEA_{100}-$UPyA_{10}$-FMA_{10} and PEA_{50}-$UPyA_{3.75}$-$FMA_{3.75}$ is 115 °C, 130 °C, 135 °C, and 115°C respectively. The PEA_{150}-$UPyA_{11.25}$-$FMA_{11.25}$ showed a decrease in

modulus at higher temperature, but no cross-over between storage and loss modulus over the plotted range of 20-150 °C. Presumably, the crossover occurs at an even higher temperature. The temperature sweep rheological data provides guidelines on how to design these IPN materials to different operating temperature for targeted applications.
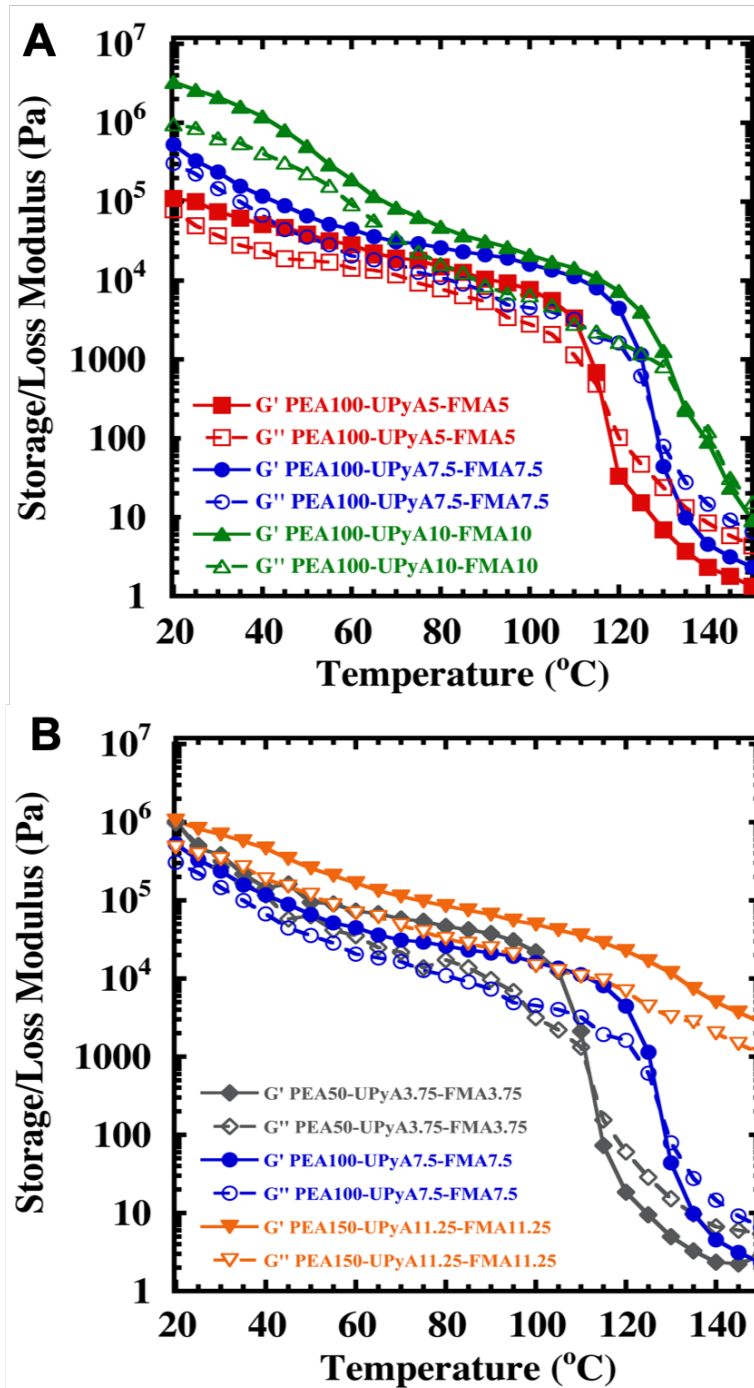
Figure 2. (A) Storage and loss modulus obtained from temperature sweep of 100 DP PEA-UPyA-FMA IPN materials in the range from 20 °C to 150 °C using 0.1% strain and 0.1 Hz. (B) Storage and loss modulus obtained from temperature sweep of PEA-UPyA-FMA IPN materials containing same molar ratio of crosslinkers while with different DP in the range from 20 °C to 150 °C using 0.1% strain and 0.1 Hz.

Dynamic properties of IPN networks

Self-Healing experiments were used to evaluate the dynamic properties of these materials, both under ambient conditions where only the hydrogen bonded UPy linkers are active, and also at elevated temperature where both UPy and Diels-Alder bonds are active. To compare IPN to other structure, a single network (SN) material was prepared, which could provide additional parameter to tune material properties comparing with IPN materials. In the SN materials, a hydroxyethyl methacrylate was used for esterification step, giving UPyMA crosslinker. Both IPN and SN materials were synthesized with the same molar ratios of the dynamic noncovalent crosslinkers (UPyMA or UPyA) and thermoresponsive furan-maleimide dynamic covalent crosslinkers and with the same degree of polymerization. Ethyl acrylate (EA) was used as the monomer to make the polymer matrix in all cases. In each system, overall molar ratio 3.75% of the UPyMA or UPyA crosslinkers and overall molar ratio of 3.75% of the furan-maleimide crosslinkers were added to the EA polymer material, resulting PEA_{100}-$UPyMA_{3.75}$-$FMA_{3.75}$ SN materials and PEA_{100}-$UPyA_{7.5}$-$FMA_{7.5}$ IPN materials. Note that the IPN and SN material are labeled according to the crosslink density in the backbone. However, the IPN material is prepared by a 1:1 mixing of UPyA containing polymer: FMA containing polymer, reducing the net crosslink density by a factor of 2. Therefore, PEA_{100}-$UPyMA_{3.75}$-$FMA_{3.75}$ SN has the same mole density of UPyA and FMA-BMI crosslinkers as the PEA_{100}-$UPyA_{7.5}$-$FMA_{7.5}$ IPN. In this way the overall composition of an IPN material and the SN material should be identical.

The PEA_{100}-$UPyA_{7.5}$-$FMA_{7.5}$ IPN and PEA_{100}-$UPyMA_{3.75}$-$FMA_{3.75}$ SN were subjected to tensile testing to break. Figure S16 shows the typical stress-strain curves of uncut as well as 1 h cold and hot self-healing properties of IPN and SN materials. The

PEA_{100}-$UPyA_{7.5}$-$FMA_{7.5}$ IPN was able to reach higher peak stress, which is around 2.0 MPa, compared to the PEA_{100}-$UPyMA_{3.75}$-$FMA_{3.75}$ SN which barely exceeded 1 MPa. This is consistent with what we discovered in our previous work when using free radical polymerization (FRP) to make SN and IPN.[48] Computational investigation has also been performed, and it was concluded that SN materials should have lower stress at break than IPN materials.[82] Since IPN architectures provide more degrees of freedom for noncovalent crosslinking to give overall stronger nonbonding interactions, the higher mechanical strength could be achieved. However, unlike architectures made by FRP, the PEA_{100}-$UPyA_{7.5}$-$FMA_{7.5}$ IPN had lower strain at break. This may be because the Diels-Alder covalent crosslinkers' distance of PEA_{100}-$UPyA_{7.5}$-$FMA_{7.5}$ IPN is nearly two times that of PEA_{100}-$UPyMA_{3.75}$-$FMA_{3.75}$ SN, which resulted in a much stiffer IPN materials.

Comparing both 1 h hot (90 °C) healed stress-strain curves, PEA_{100}-$UPyA_{7.5}$-$FMA_{7.5}$ IPN had better self-healing property. As indicated in Figure S16, PEA_{100}-$UPyA_{7.5}$-$FMA_{7.5}$ IPN could give approximately ~70% recovery in the strain at break and ~60% recovery in the peak stress after heating at 90 °C for 1 h, while PEA_{100}-$UPyMA_{3.75}$-$FMA_{3.75}$ SN could only give approximately ~45% recovery in the both strain at break and peak stress. The best healing performance of PEA_{100}-$UPyA_{7.5}$-$FMA_{7.5}$ IPN in the strain at break was ~57%, and the peak stress was ~40% of the original material tensile properties at room temperature, while the PEA_{100}-$UPyMA_{3.75}$-$FMA_{3.75}$ SN could give approximately ~32% recovery in the strain at break and ~55% recovery in the peak stress. Our previous work also showed that when using static divinylbenzene (DVB) as the only crosslinker in RAFT based PEA materials, the

materials had negligible self-healing ability.[49] This shows that the dynamic UPyA and Diels-Alder bonds are needed for the observed self-healing.

The self-healing properties of all five kinds of IPN materials were explored. Figures S17-S19, Figure 3 and Figure 4 compare the stress-strain curves of all the IPN uncut material, and also the stress-strain curves for a material that was cut in half, and reattached by pushing the two parts together, followed by incubation at ambient temperature or at 90 °C for different times. The best performing materials were taken to represent their self-healing properties and compares to uncut materials. Figure 3A and 3B shows that the PEA_{100}-$UPyA_{7.5}$-$FMA_{7.5}$ IPN materials are able to recover a significant proportion of the original mechanical properties. In fact, the best healing performance of PEA_{100}-$UPyA_{7.5}$-$FMA_{7.5}$ IPN in the peak stress was ~40%, and the strain at break was ~57% of the original material tensile properties at room temperature. At 90 °C, the best healing performance in the peak stress was ~85%, and the strain at break was ~95% of the original material tensile properties. The IPN materials that were self-healed for 1 h cold were similar to earlier timepoints, indicating a plateau of material recovery. Similarly, 7h was sufficient to essentially reach a plateau of self-healing under heated conditions. As shown in Figure 3A, even the 30 min cold healing performed similarly with the 1 hour's. Similarly, Figure 3B shows that the 4 h hot healing performed similarly with the 7-hour sample. Overall, the self-healing ability at 90 °C outperformed the self-healing ability at ambient temperature when the healing time periods is above 30 min. This can be due to two reasons. In general, elevated temperature accelerate all kinetic exchange processes. Further, the dynamic covalent Diels-Alder adducts require thermal stimulus to activate the dynamic covalent exchange, hence samples

heated to 90 °C are able to exchange and reform both hydrogen bonded UPyA and also Diels-Alder FMA-BMI crosslinkers.
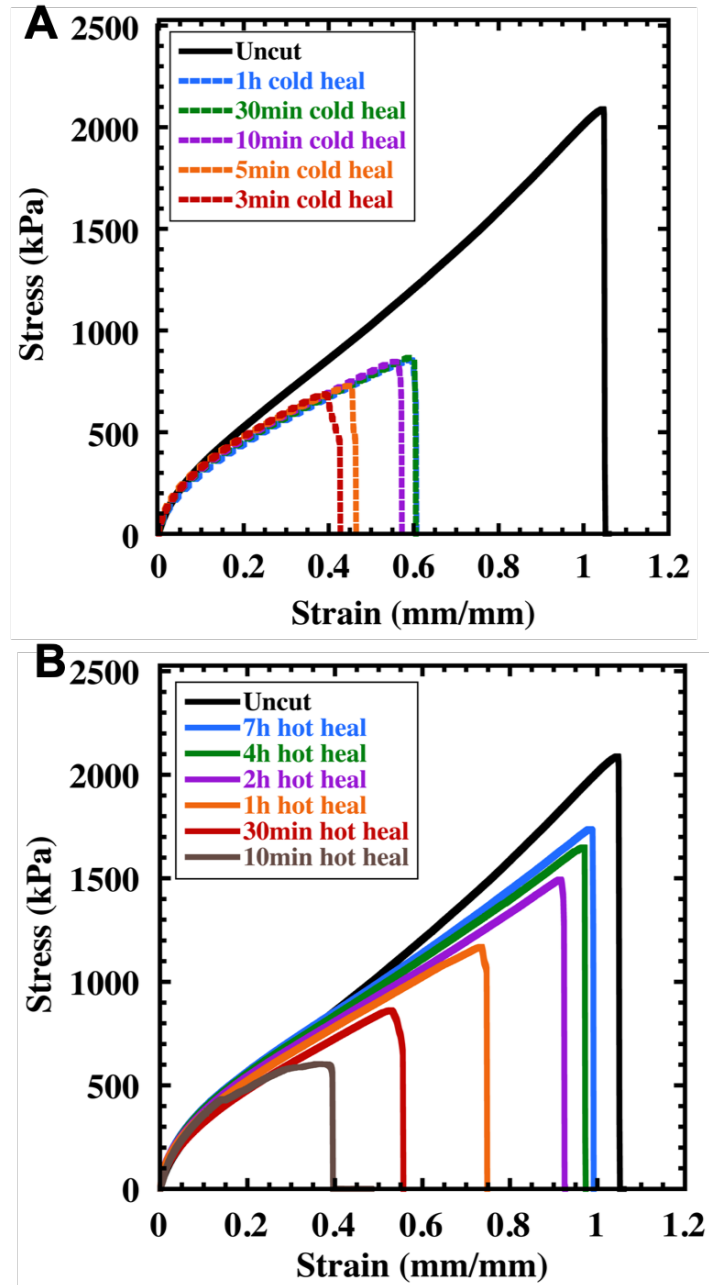

Figure 3. Self-healing properties. (A) Typical stress vs strain curves after different healing time for cold heal of PEA$_{100}$-UPyA$_{7.5}$-FMA$_{7.5}$ IPN materials at room temperature. (B) Typical stress vs strain curves after different healing time for hot heal of PEA$_{100}$-UPyA$_{7.5}$-FMA$_{7.5}$ IPN materials at 90 °C.

The extensive range of materials developed here suggest that the material's healing properties are inversely proportional to the content of the crosslinker or the degree of polymerization, both at ambient environment or elevated temperature. Comparing the various IPN materials, the PEA_{100}-$UPyA_5$-FMA_5 IPN, has the best self-healing performance among these three materials at both room and elevated temperature, as seen in Figure 4. The recovery of PEA_{100}-$UPyA_5$-FMA_5 IPN at 90°C is up to 100% shown in Figure 4B and 4D, because all of the samples, which were cut in the middle and heated after different time lengths, broke in a place completely separate from the original fracture site, behaving just like the uncut materials. Interestingly, even 10 min of heating at 90°C led to essentially complete recovery of mechanical properties and no measurable differentiation between the uncut PEA_{100}-$UPyA_5$-FMA_5 IPN and the sample healed at 90°C for 10 min. The original scratches in the middle were barley seen after being heated only 10 min. This enables the polymer to have potential applications as an innovative coating material possessing efficient self-healing ability in the future.
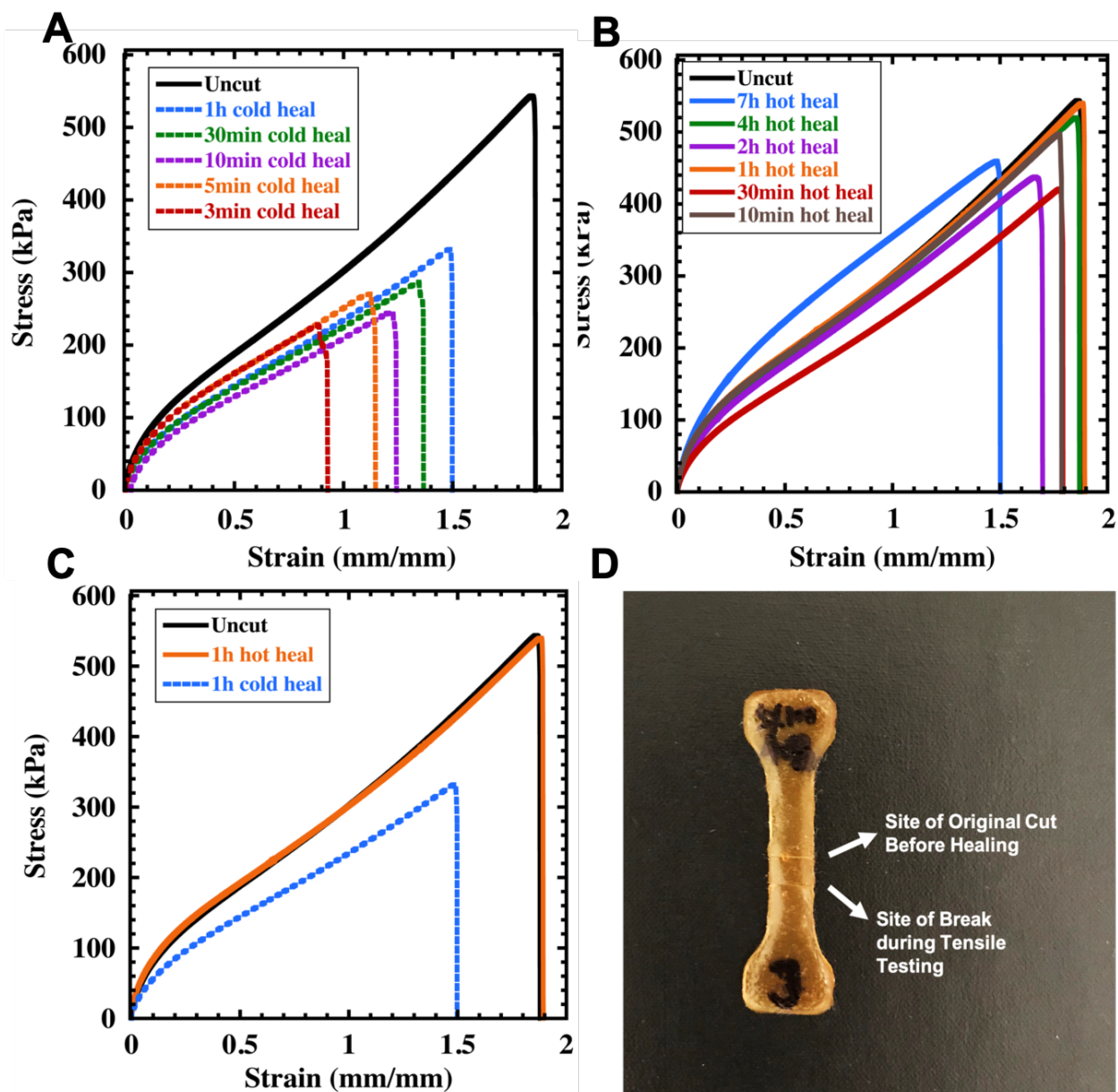
Figure 4. Self-healing properties of PEA$_{100}$-UPyA$_5$-FMA$_5$ IPN materials. (A) Typical stress vs strain curves after different healing time for cold heal of PEA$_{100}$-UPyA$_5$-FMA$_5$ IPN at room temperature. (B) Typical stress vs strain curves after different healing time for hot heal of PEA$_{100}$-UPyA$_{7.5}$-FMA$_{7.5}$ IPN at 90 °C. (C) Comparison of 1 h hot heal stress-strain curve with 1 h cold heal stress-strain curve. (D) Photograph of a PEA$_{100}$-UPyA$_5$-FMA$_5$ IPN indicating site of original cut and break point during mechanical testing after 10 min of healing at 90 °C.

The same phenomenon was observed when testing the self-healing ability of PEA$_{50}$-UPyA$_{3.75}$-FMA$_{3.75}$ at 90 °C as shown in Figure S18B and S18D. PEA$_{100}$-UPyA$_{10}$-FMA$_{10}$ IPN and PEA$_{150}$-UPyA$_{11.25}$-FMA$_{11.25}$ IPN showed negligible self-healing properties at

ambient temperature and only have limited self-healing abilities at 90 °C. This could be due to two factors. One observation for the PEA_{100}-$UPyA_{10}$-FMA_{10} IPN and PEA_{150}-$UPyA_{11.25}$-$FMA_{11.25}$ IPN materials was that they are not sticky to touch, owning to their stiffness. However, PEA_{100}-$UPyA_5$-FMA_5 IPN, PEA_{100}-$UPyA_{7.5}$-$FMA_{7.5}$ IPN and PEA_{50}-$UPyA_{3.75}$-$FMA_{3.75}$ IPN had the two ends stick together effectively as soon as the two ends were placed in contact. The other reason is that with the higher crosslinker content and longer chain length, the polymer chains are less mobile, leading to the broken dynamic bonds having lower probability to find its counterparts in a given time frame. This is likely because with higher crosslink density or longer chains multiple dynamic bonds need to dissociate in order to allow chains to diffuse and reattach for effective healing.

The tendency of dynamic crosslinked materials to creep under load is a significant limitation toward applications.[6] Therefore, the stability of all the PEA-UPyA-FMA IPN materials were explored. The long-term stability of these materials was tested under strain and stress. Figure 5A shows the stress relaxation at 25% average ε_{break} for each material. The performances of stress relaxation for all the PEA-UPyA-FMA IPN materials are regarded as being essentially the same. The degree of stress relaxation was approximately 95% of the initial stress due to the unrestricted hydrogen bonds which could dissipate most of the stress by rearranging and dissociating followed by reassociation. All samples required just 2 h to reach the plateau, suggesting that all the IPN materials can resist the deformation eventually, since the stress relaxation is effective but limited. Figure S20 shows the result of creep deformation tests. All the IPN materials except PEA_{100}-$UPyA_5$-FMA_5 IPN were tested with an applied stress of 50 kPa. However, the complete creep recovery was not observed in any kinds of IPN materials in 2 h. Complementary to the stress

relaxation and creep deformation experiments, all the IPN materials were subjected to long-term stability studies. All materials were strained to 25% of the average ε_{break} and fixed at ambient temperature. After 24 h, the strain was released. The materials were allowed to recover and measured at different timepoints as shown in Figure 5B. All the IPN materials restored to their original length eventually. PEA_{100}-$UPyA_{10}$-FMA_{10} IPN and PEA_{150}-$UPyA_{11.25}$-$FMA_{11.25}$ IPN were much faster which only took 4 h. PEA_{100}-$UPyA_5$-FMA_5 IPN, PEA_{100}-$UPyA_{7.5}$-$FMA_{7.5}$ IPN and PEA_{50}-$UPyA_{3.75}$-$FMA_{3.75}$ IPN took 2-7 days to restore to their original shape. This is due to the FMA-BMI Diels-Alder adducts being unable to exchange under ambient conditions, leading to the permanent shape being retained at ambient conditions.
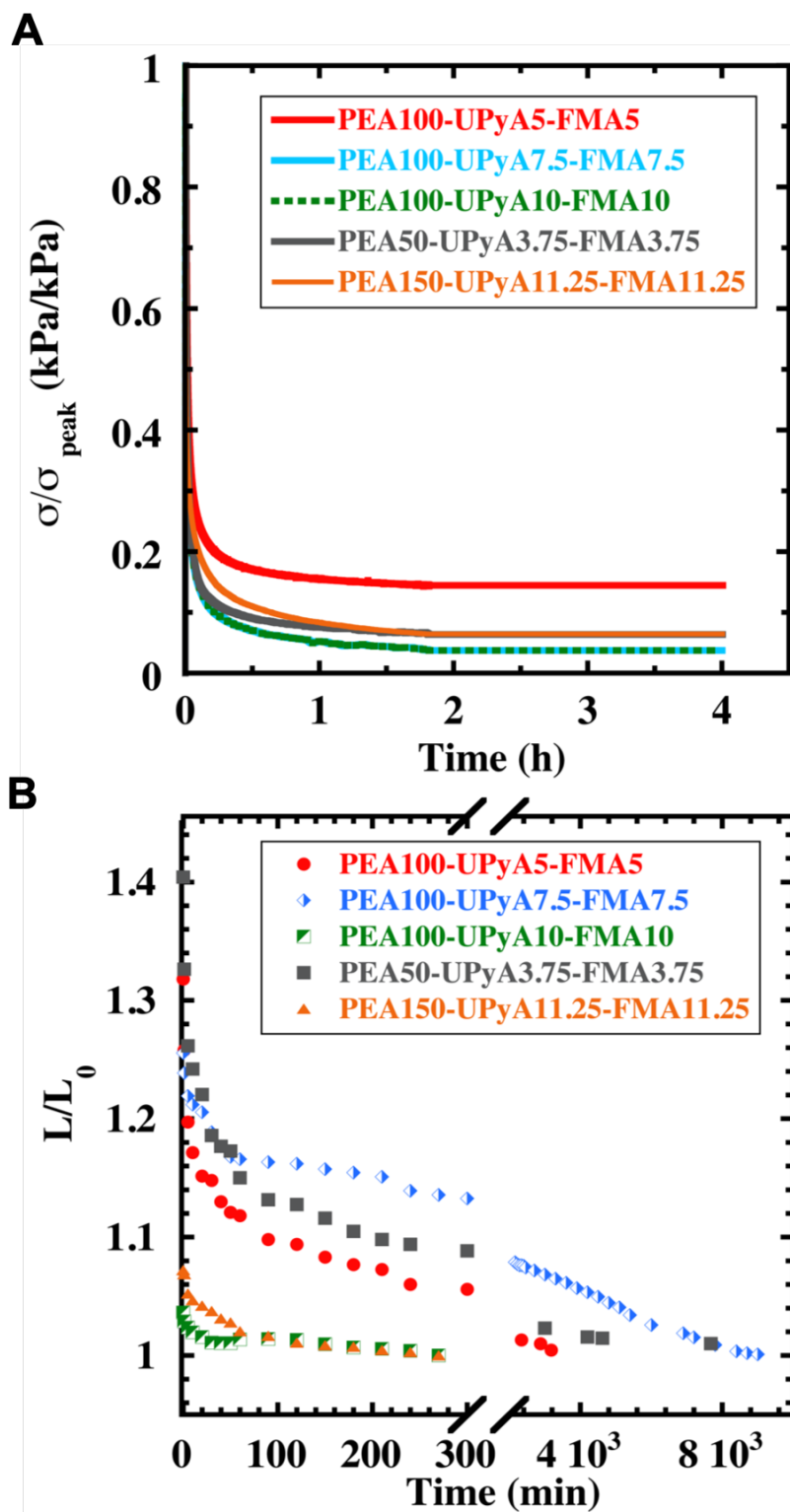
Figure 5. (A) Stress relaxation of all the PEA-UPyA-FMA IPN materials. The material was strained to the 25% average strain at break. (B) Creep recovery as a function of time for all the PEA-UPyA-FMA IPN materials after being released from the 25% average strain at break. Both studies were performed at ambient temperature.

The results of stress relaxation and creep deformation tests suggested that these IPN materials may have very good malleability. This is consistent with the concept that dynamic materials have reshaping ability or malleability when strained under conditions that favor the exchange of the dynamic bonds. The exchange of the dynamic bonds enables a release of the stress induced by the applied strain, with a change in the permanent shape of the dynamic materials. Therefore, PEA_{100}-$UPyA_{7.5}$-$FMA_{7.5}$ IPN material was chosen to investigate the malleability. The tests were performed at 90 °C for different time length and the angles were measured at each timepoint. Figure 6 shows the malleability of PEA_{100}-$UPyA_{7.5}$-$FMA_{7.5}$ IPN material. It is found that the twisted configuration of PEA_{100}-$UPyA_{7.5}$-$FMA_{7.5}$ IPN material increased as time raise. 100% of the target 360° was achieved only in 1 h. This malleability could enable the material to be a scaffold for shape memory applications.
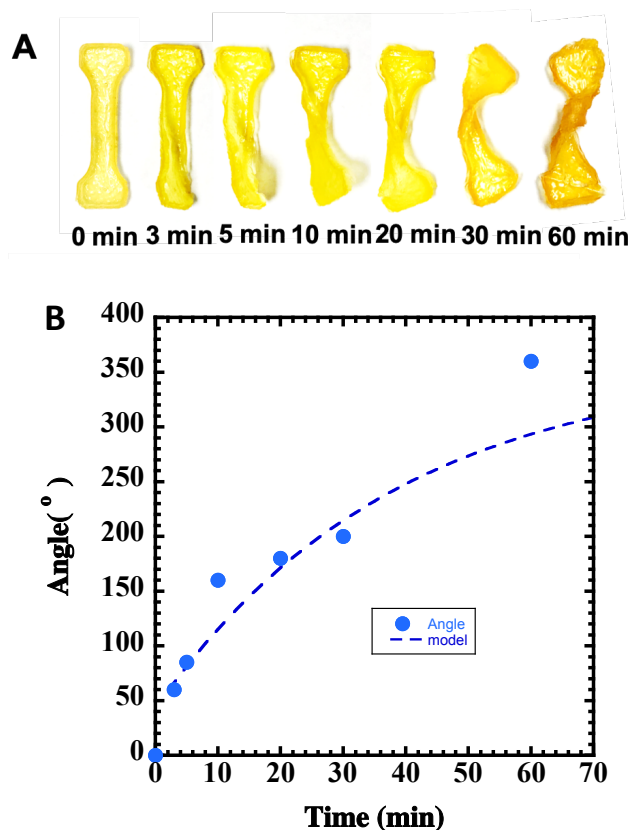

A

0 min 3 min 5 min 10 min 20 min 30 min 60 min

B

Angle(°)

Time (min)

● Angle
-- model

Figure 6. (A)Photograph of the new shape of the PEA$_{100}$-UPyA$_{7.5}$-FMA$_{7.5}$ IPN materials after fixed 360° at 90°C for different time lengths and then fully relaxed. (B) Malleability of PEA$_{100}$-UPyA$_{7.5}$-FMA$_{7.5}$ IPN material at different times at 90 °C. Malleability data was fit with the function angle = 360-318 exp(-0.026 time), where time is measured in minutes.

Simulations of Polymer Networks

Finally, course grained molecular dynamics (MD) simulations were performed, similar to those developed by our group,[82] to understand the performance of the materials. In these course grained simulations each monomer was approximated as a bead, with UPyA and FMI-BMA approximated as multiple beads connected together. Importantly, the backbone forming beads (blue spheres) were assumed to only have short range repulsive interactions since they have no hydrogen bond donors, while each hydrogen bonding unit in UPyA was approximated as having a bond energy of 1 k$_B$T. The covalent bonds were modeled as harmonic bonds within the MD simulations with a harmonic bond constant assumed to require a high energy of 10 k$_B$T to double the initial bond length. MD simulations were conducted using the LAMMPS software package[94] in the NVT ensemble, using a time step of *90ps* and a temperature of *T = 300 K.* The system used for the simulations is given in Figure 7A. The simulated stress strain curves for PEA$_{100}$-UPyA$_{7.5}$-FMA$_{7.5}$ IPN and PEA$_{100}$-UPyMA$_{3.75}$-FMA$_{3.75}$ SN materials is given in Figure 7B. The simulations were able to replicate the higher peak stress of the IPN material, although they suggested that the SN material should have a lower strain at break, in contrast to the experimental data. Differences between the simulated and experimental ε_{break} is most likely due to the coarse graining used in the simulations. Nevertheless, the simulations accurately capture the trend in σ_{peak} for the IPN and SN materials. Importantly, the higher σ_{peak} and toughness is due to increased number of non-

covalent bonds in the IPN material compared to the SN, due to the increased freedom of the IPN hydrogen bonded network.
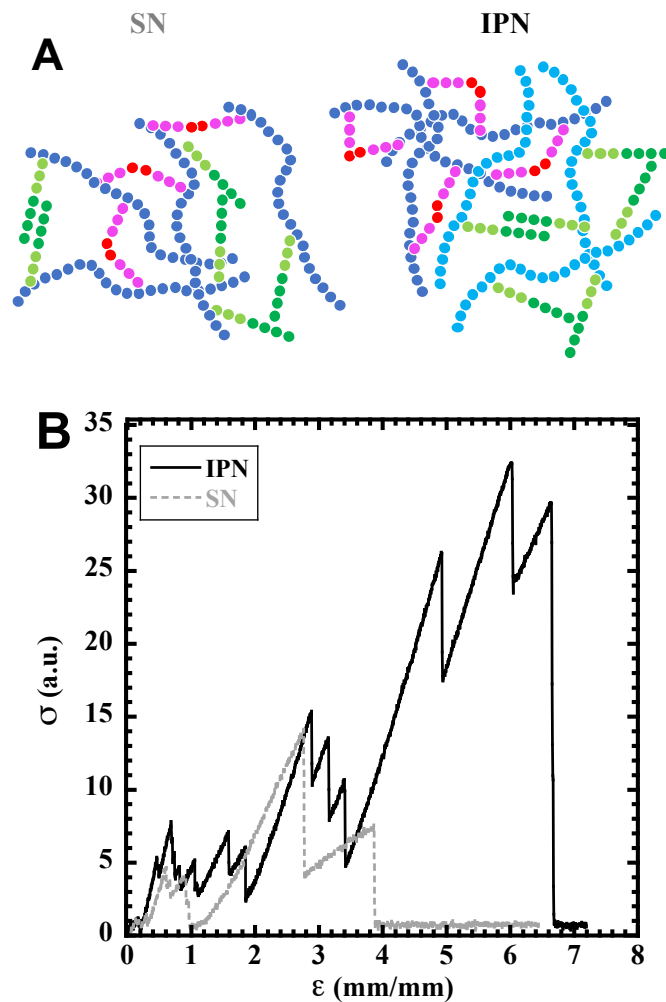

Figure 7. A) Schematic of chains used in MD simulations. Blue represents polymer backbone forming monomer, green represents hydrogen bonded UPyA and red represents FMA-BMI adducts. B) Simulated stress strain curves for PEA$_{100}$-UPyA$_{7.5}$-FMA$_{7.5}$ IPN and PEA$_{100}$-UPyMA$_{3.75}$-FMA$_{3.75}$ SN materials.

Conclusions

Well-defined polymers containing hydrogen bonded UPyA units and dynamic covalent furan-maleimide based crosslinkers were synthesized by RAFT polymerization. This approach allows polymer microstructure to be precisely

engineered and designed. In general, higher crosslink densities led to stronger materials that were less elastic. Similarly, long chain lengths led to substantially stronger and less elastic materials. The materials generally showed a rheological crossover temperature in the range of 110-135 °C, changing from elastic below the crossover temperature and viscous above that temperature. The only exception was the material with 7.5mol% crosslinker in each network with a chain length of 150 units, which didn't cross over in the studied temperature range. All IPN materials showed self-healing characteristics, with an inverse correlation of chain length, cross-linker density and self-healing efficiency. The self-healing of the IPN material was more efficient than a comparable SN material with the SN material able to withstand lower stresses before breaking. This is likely because the materials with shorter chain lengths and lower crosslink densities have more mobile chains which are able to exchange more rapidly. Finally, all IPN materials relax stresses very efficiently due to exchange of H bonded UPyA units, although they are resistant to permanent creep under the same conditions. With these fundamental studies in hand, the materials developed serve as an excellent platform for the development of coatings, sealants, elastomers or adhesives with self-healing properties.

Conflicts of interest

There are no conflicts to declare

Acknowledgements

References

1.   P. T. Corbett, J. Leclaire, L. Vial, K. R. West, J.-L. Wietor, J. K. M. Sanders and S. Otto, *Chem. Rev.*, 2006, **106**, 3652-3711.
2.   J.-M. Lehn and A. V. Eliseev, *Science*, 2001, **291**, 2331-2332.
3.   J.-M. Lehn, *Prog. Polym. Sci.*, 2005, **30**, 814-831.
4.   J.-Y. Sun, X. Zhao, W. R. K. Illeperuma, O. Chaudhuri, K. H. Oh, D. J. Mooney, J. J. Vlassak and Z. Suo, *Nature*, 2012, **489**, 133-136.
5.   N. Roy, E. Buhler and J. M. Lehn, *Polym. Int.*, 2014, **63**, 1400-1405.
6.   N. Roy, B. Bruchmann and J.-M. Lehn, *Chem. Soc. Rev.*, 2015, **44**, 3786-3807.
7.   P. Chakma and D. Konkolewicz, *Angew. Chem. Int Ed.*, 2019, **58**, 9682-9695.
8.   E. Kolomiets and J.-M. Lehn, *Chem. Commun.*, 2005, 1519-1521.
9.   S. Burattini, B. W. Greenland, D. H. Merino, W. Weng, J. Seppala, H. M. Colquhoun, W. Hayes, M. E. Mackay, I. W. Hamley and S. J. Rowan, *J. Am. Chem. Soc.*, 2010, **132**, 12051-12058.
10.   M. Burnworth, L. Tang, J. R. Kumpfer, A. J. Duncan, F. L. Beyer, G. L. Fiore, S. J. Rowan and C. Weder, *Nature*, 2011, **472**, 334.
11.   X. Yan, F. Wang, B. Zheng and F. Huang, *Chem. Soc. Rev.*, 2012, **41**, 6042-6065.
12.   Y. Yang and M. W. Urban, *Chem. Soc. Rev.*, 2013, **42**, 7446-7467.
13.   D. Mozhdehi, S. Ayala, O. R. Cromwell and Z. Guan, *J. Am. Chem. Soc.*, 2014, **136**, 16128-16131.
14.   H. Liu, C. Xiong, Z. Tao, Y. Fan, X. Tang and H. Yang, *RSC Adv.*, 2015, **5**, 33083-33088.
15.   S. Monemian and L. T. Korley, *Macromolecules*, 2015, **48**, 7146-7155.
16.   Y. Hu, W. Han, G. Huang, W. Zhou, Z. Yang and C. Wang, *Macromol. Chem. Phys.*, 2016, **217**, 2717-2725.
17.   Z. Wang, Y. Ren, Y. Zhu, L. Hao, Y. Chen, G. An, H. Wu, X. Shi and C. Mao, *Angew. Chem. Int Ed.*, 2018, **57**, 9008-9012.
18.   Y. Yang and M. W. Urban, *Adv. Mater. Interf.*, 2018, **5**, 1800384.
19.   M. Mauro, *Eur. J. Inorg. Chem.*, 2018, **2018**, 2090-2100.
20.   S. J. Rowan, S. J. Cantrill, G. R. Cousins, J. K. Sanders and J. F. Stoddart, *Angew. Chem. Int. Ed.*, 2002, **41**, 898-952.
21.   P. J. Boul, P. Reutenauer and J.-M. Lehn, *Org. Lett.*, 2005, **7**, 15-18.
22.   T. Maeda, H. Otsuka and A. Takahara, *Prog. Polym. Sci.*, 2009, **34**, 581-604.
23.   J. W. Chan, C. E. Hoyle, A. B. Lowe and M. Bowman, *Macromolecules*, 2010, **43**, 6381-6388.
24.   C. E. Hoyle, A. B. Lowe and C. N. Bowman, *Chem. Soc. Rev.*, 2010, **39**, 1355-1387.

25. H. Otsuka, S. Nagano, Y. Kobashi, T. Maeda and A. Takahara, *Chem. Commun.*, 2010, **46**, 1150-1152.

26. G. Hizal, U. Tunca and A. J. Sanyal, *J. Polym. Sci. Part A: Polym. Chem.*, 2011, **49**, 4103-4120.

27. M. E. Belowich and J. F. Stoddart, *Chem. Soc. Rev.*, 2012, **41**, 2003-2024.

28. S. P. Black, J. K. Sanders and A. R. Stefankiewicz, *Chem. Soc. Rev.*, 2014, **43**, 1861-1872.

29. S. Chatani, T. Gong, B. A. Earle, M. Podgorski and C. N. Bowman, *ACS Macro Lett.*, 2014, **3**, 315-318.

30. S. D. Fontaine, R. Reid, L. Robinson, G. W. Ashley and D. V. Santi, *Bioconj. Chem.*, 2014, **26**, 145-152.

31. S.-H. Guo, S.-Z. Xing, S. Mao, Y.-R. Gao, W.-L. Chen and Y.-Q. Wang, *Tetrahedron Lett.*, 2014, **55**, 6718-6720.

32. J. Chen, X. Jiang, S. L. Carroll, J. Huang and J. Wang, *Org. Lett.*, 2015, **17**, 5978-5981.

33. F. García and M. M. Smulders, *J. Polym. Sci. Part A: Polym. Chem.*, 2016, **54**, 3551-3577.

34. D. E. Apostolides and C. S. Patrickios, *Polym Int*, 2018, **67**, 627-649.

35. J. J. Cash, T. Kubo, D. J. Dobbins and B. S. Sumerlin, *Polym. Chem.*, 2018, **9**, 2011-2020.

36. Y. Jin, Q. Wang, P. Taynton and W. Zhang, *Acc. Chem. Res.*, 2014, **47**, 1575-1586.

37. Y. Jin, C. Yu, R. J. Denman and W. Zhang, *Chem. Soc. Rev.*, 2013, **42**, 6634-6654.

38. H. A. Khan, K. G. Kou and V. M. Dong, *Chem. Sci.*, 2011, **2**, 407-410.

39. N. Kuhl, S. Bode, R. K. Bose, J. Vitz, A. Seifert, S. Hoeppener, S. J. Garcia, S. Spange, S. van der Zwaag and M. D. Hager, *Adv. Funct. Mater.*, 2015, **25**, 3295-3301.

40. N. Kuhl, R. Geitner, J. Vitz, S. Bode, M. Schmitt, J. Popp, U. S. Schubert and M. D. Hager, *J. Appl. Polym. Sci.*, 2017, **134**, 44805.

41. B. H. Northrop, S. H. Frayne and U. Choudhary, *Polym. Chem.*, 2015, **6**, 3415-3430.

42. R. J. Wojtecki, M. A. Meador and S. J. Rowan, *Nat. Mater.*, 2011, **10**, 14-27.

43. P. Wang, G. Deng, L. Zhou, Z. Li and Y. Chen, *ACS Macro Lett.*, 2017, **6**, 881-886.

44. B. Zhang, Z. A. Digby, J. A. Flum, P. Chakma, J. M. Saul, J. L. Sparks and D. Konkolewicz, *Macromolecules*, 2016, **49**, 6871-6878.

45. W. Zhang and Y. Jin, *Dynamic Covalent Chemistry: Principles, Reactions, and Applications*, John Wiley & Sons, 2017.

46. B. Zhang, Z. A. Digby, J. A. Flum, E. M. Foster, J. L. Sparks and D. Konkolewicz, *Polym. Chem.*, 2015, **6**, 7368-7372.

47. F. Sordo, S. b.-J. Mougnier, N. Loureiro, F. o. Tournilhac and V. r. Michaud, *Macromolecules*, 2015, **48**, 4394-4402.

48. E. M. Foster, E. E. Lensmeyer, B. Zhang, P. Chakma, J. A. Flum, J. J. Via, J. L. Sparks and D. Konkolewicz, *ACS Macro Lett.*, 2017, **6**, 495-499.

49. P. Chakma, Z. A. Digby, J. Via, M. P. Shulman, J. L. Sparks and D. Konkolewicz, *Polym. Chem.*, 2018, **9**, 4744-4756.

50. A. Wilson, G. Gasparini and S. Matile, *Chem. Soc. Rev.*, 2014, **43**, 1948-1962.

51. A. M. Kushner, V. Gabuchian, E. G. Johnson and Z. Guan, *J. Am. Chem. Soc.*, 2007, **129**, 14110-14111.

52. C. E. Diesendruck, N. R. Sottos, J. S. Moore and S. R. White, *Angew. Chem. Int Ed.*, 2015, **54**, 10428-10447.

53. E. Ducrot, Y. Chen, M. Bulters, R. P. Sijbesma and C. Creton, *Science*, 2014, **344**, 186-189.

54.   X. Zhou, B. Guo, L. Zhang and G.-H. Hu, *Chem. Soc. Rev.*, 2017, **46**, 6301-6329.
55.   L. Brunsveld, B. Folmer, E. W. Meijer and R. Sijbesma, *Chem. Rev.*, 2001, **101**, 4071-4098.
56.   J. Cui and A. D. Campo, *Chem. Comm.*, 2012, **48**, 9302.
57.   M. Guo, L. M. Pitet, H. M. Wyss, M. Vos, P. Y. Dankers and E. Meijer, *J. Am. Chem. Soc.*, 2014, **136**, 6969-6977.
58.   M. A. Tasdelen, *Polym. Chem.*, 2011, **2**, 2133.
59.   S. Li, L. Wang, X. Yu, C. Wang and Z. Wang, *Mater Sci. Eng.: C*, 2018, **82**, 299-309.
60.   C. Xiao, Y. Zhu, J. Chen and S. Zhang, *Polymer*, 2017, **110**, 74-79.
61.   S. J. Garcia, *Eur. Polym. J.*, 2014, **53**, 118-125.
62.   G. Moad, Y. Chong, A. Postma, E. Rizzardo and S. H. Thang, *Polymer*, 2005, **46**, 8458-8468.
63.   D. Konkolewicz, A. Gray-Weale and S. Perrier, *Polym. Chem.*, 2010, **1**, 1067-1077.
64.   A. E. Smith, X. Xu and C. L. McCormick, *Prog. Polym. Sci.*, 2010, **35**, 45-93.
65.   D. Konkolewicz, C. K. Poon, A. Gray-Weale and S. Perrier, *Chem. Commun.*, 2011, **47**, 239-241.
66.   Y. Ma, J.-F. Gao, C. Zheng and H. Zhang, *J. Mater. Chem. B*, 2019, **7**, 2474-2483.
67.   J. Chiefari, Y. Chong, F. Ercole, J. Krstina, J. Jeffery, T. P. Le, R. T. Mayadunne, G. F. Meijs, C. L. Moad and G. Moad, *Macromolecules*, 1998, **31**, 5559-5562.
68.   A. W. Jackson and D. A. Fulton, *Macromolecules*, 2009, **43**, 1069-1075.
69.   P. De, S. R. Gondi, D. Roy and B. S. Sumerlin, *Macromolecules*, 2009, **42**, 5614-5621.
70.   G. Moad, *Polym. Chem.*, 2017, **8**, 177-219.
71.   E. G. Wilborn, C. M. Gregory, C. A. Machado, T. M. Page, W. Ramos, M. A. Hunter, K. M. Smith, S. E. Gosting, R. Tran and K. L. Varney, *Macromolecules*, 2019, **52**, 1308-1316.
72.   J.-F. Xu, Y.-Z. Chen, L.-Z. Wu, C.-H. Tung and Q.-Z. Yang, *Org. Lett.*, 2013, **15**, 6148-6151.
73.   J. Liu, Y. Liu, Y. Wang, J. Zhu, J. Yu and Z. Hu, *Mater. Today Commun.*, 2017, **13**, 282-289.
74.   Y. Wang, H. Yu, H. Yang, X. Hao, Q. Tang and X. Zhang, *Macromol. Chem. Phys.*, 2017, **218**, 1700348.
75.   Y. Peng, Y. Yang, Q. Wu, S. Wang, G. Huang and J. Wu, *Polymer*, 2018, **157**, 172-179.
76.   K. Sugane, R. Takagi and M. Shibata, *React. Funct. Polym.*, 2018, **131**, 211-218.
77.   B. Zhou, C. Zuo, Z. Xiao, X. Zhou, D. He, X. Xie and Z. Xue, *Chem. Eur. J.*, 2018, **24**, 19200-19207.
78.   Z. Zhuang, L. Wu, X. Ma, W. Diao and Y. Fang, *J. Appl. Polym. Sci.*, 2018, **135**, 46847.
79.   Y. A. Wang, H. S. Yu, H. Y. Yang, X. Hao, Q. Tang and X. Y. Zhang, *Macromol. Chem. Phys.*, 2017, **218**, 8.
80.   Z. H. Tang, X. L. Lyu, A. Q. Xiao, Z. H. Shen and X. H. Fan, *Chem. Mater.*, 2018, **30**, 7752-7759.
81.   L. W. Zhou, T. J. Ma, T. T. Li, X. D. Ma, J. Yin and X. S. Jiang, *ACS Appl. Mater. Interfaces*, 2019, **11**, 15977-15985.
82.   M. B. Zanjani, B. Zhang, B. Ahammed, J. P. Chamberlin, P. Chakma, D. Konkolewicz and Z. Ye, *Macromol Theory Simul.*, 2019, DOI: 10.1002/mats.201900008, 1900008.
83.   H. M. Keizer, R. van Kessel, R. P. Sijbesma and E. Meijer, *Polymer*, 2003, **44**, 5505-5511.
84.   2004.
85.   T. Lee, B. Kim, S. Kim, J. H. Han, H. B. Jeon, Y. S. Lee and H.-j. Paik, *Nanoscale*, 2015, **7**, 6745-6753.

86.   C. J. Ferguson, R. J. Hughes, D. Nguyen, B. T. Pham, R. G. Gilbert, A. K. Serelis, C. H. Such and B. S. Hawkett, *Macromolecules*, 2005, **38**, 2191-2204.

87.   A. F. Craig, E. E. Clark, I. D. Sahu, R. Zhang, N. D. Frantz, M. S. Al-Abdul-Wahid, C. Dabney-Smith, D. Konkolewicz and G. A. Lorigan, *Biochim. Biophys. Acta*, 2016, **1858**, 2931-2939.

88.   O. A. Shergold, N. A. Fleck and D. Radford, *Int. J. Impact Eng.*, 2006, **32**, 1384-1402.

89.   G. Gody, P. B. Zetterlund, S. Perrier and S. Harrisson, *Nat. Commun.*, 2016, **7**, 10514.

90.   Y. Amamoto, H. Otsuka, A. Takahara and K. Matyjaszewski, *Adv Mater*, 2012, **24**, 3975-3980.

91.   F. Chambon, Z. S. Petrovic, W. J. Macknight and H. H. Winter, *Macromolecules*, 1986, **19**, 2146-2149.

92.   J. D. Ferry, *Viscoelastic properties of polymers*, John Wiley & Sons, 1980.

93.   D. Roylance, *Department of Materials Science and Engineering–Massachusetts Institute of Technology, Cambridge MA*, 2001, **2139**, 1-37.

94.   S. Plimpton, P. Crozier and A. Thompson, *Sandia National Laboratories*, 2007, **18**, 43.
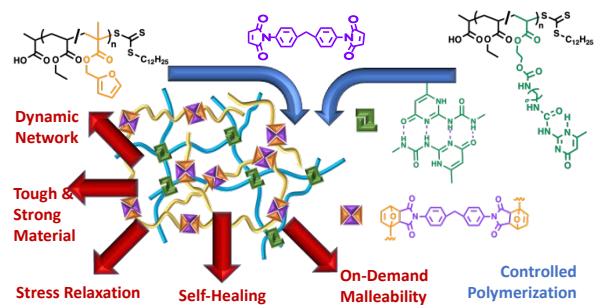
Controlled polymerization is used to make well defined polymers that are assembled into dynamic interpenetrated network materials. Self-healing, toughness and stress relaxation are imparted into the material through the dynamic linkages.